

Low-Profile Microstrip Patch Antenna for Over-Body Surface Communication at 2.45 GHz

Gareth A. Conway, William G. Scanlon, *Member, IEEE* and D. Linton, *Senior Member, IEEE*

Abstract—A compact higher-order mode microstrip patch antenna (HM-MPA) suitable for on-body communications at 2.45 GHz is presented. Using FDTD simulations we show that the HM-MPA had an impedance bandwidth of 150 MHz and a relatively good bodyworn efficiency of more than 60 % when placed in close proximity to a lossy medium with the characteristics of muscle tissue. On-body performance was investigated by modelling S_{21} coupling of two HM-MPAs spaced 200 mm apart on a muscle tissue layer. The HM-MPA coupling results are comparable to those achieved using a quarter wave monopole antenna on the same size of groundplane, mounted normal to the tissue surface. Considering that the HM-MPA has the benefit of being low-profile and physically more robust, it is a promising solution for over body surface applications.

Index Terms—Wearable antennas; human body effects; compact patch antenna; on-body communications.

I. INTRODUCTION

Wireless technologies for bodyworn applications are still in the early stages of development. Government, military and medical sectors are providing the momentum behind the majority of research initiatives for the development and deployment of wearable communication systems. Emerging military applications are focused on integrating these devices into military clothing in an attempt to enhance soldier performance, awareness and survivability on the battle field [1]. Recently, biomedical sensor networks mounted on or implanted within the human body have drawn greater attention for healthcare monitoring. As populations grow and age, the demand on health care resources increases and many governments are looking for remote healthcare solutions. Wearable monitoring systems have the capability to monitor medical data in the home or ward, facilitating disease prediction, diagnosis and, in some cases, even control of the condition. By reducing clinician face-to-face consultations and shortening hospital stays, such technology can help compensate for limited health care resources. Regardless of the application area, an important aspect of wearable communications is the preservation of antenna performance, yet antennas must be small, unobtrusive to the user and, ideally conformable to the body surface.

To date there has been no significant breakthrough in the design of low-profile body-mounted antennas but studies of body-worn or wearable antennas have recently received much attention [2]–[5]. One design option is the use of flexible substrates such as textile materials to achieve a low-profile solution [6]. Such fabric antennas are more prone to

discontinuities in substrate material and manufacturing related performance variations in comparison to antennas constructed using available high-quality rigid substrates. Secure feed connection to textile antennas remains a significant problem in robust wearable system design.

It is widely accepted that antenna performance is significantly affected by close proximity to the human body. For example, radiation pattern fragmentation (varying propagation conditions), reduced radiation efficiency due to bulk power absorption, resonant frequency shift (antenna detuning) and changes in antenna input impedance due to antenna-body capacitive coupling are commonly reported [7]. Furthermore, the effect of the user's body on antenna characteristics are largely due to the amount of antenna-body coupling and will vary between different antennas, separation distances and near-field coupling with tissue.

Printed antennas offer favourable characteristics such as low-profile, low-cost, conformability and often ease of manufacture. Therefore, such antennas are strong candidates for use for wearable applications at frequencies above 1 GHz where their dimensions become manageable for most bodyworn applications. The changes in printed antenna characteristics when in close proximity to a lossy medium have been reported in the literature [2]. Furthermore, because of increased antenna-body coupling these effects are further compounded when antennas are mounted on small ground planes. However, in wearable applications antenna size is typically a critical design criterion and hence ground plane dimensions need to be minimized as much as possible.

Therefore, in this paper we present a higher-mode microstrip patch antenna (HM-MPA) with a relatively small (0.25λ) ground plane that has promising characteristics for over the body surface communication (known as an 'on-body' channel). We report simulated S_{21} coupling performance for the HM-MPA in close proximity to a lossy medium representing body tissues. The results are compared to a quarter wave monopole antenna on the same size of ground plane, mounted normal to the tissue surface. This is the first time that a higher-mode microstrip antenna has been studied in close proximity to lossy materials representative of the on-body environment. All simulated results in this work were obtained with the SEMCAD X (Schmid & Partner Engineering AG, Zürich, Switzerland) finite-difference time-domain (FDTD) electromagnetic numerical modelling platform.

II. ON-BODY CHANNEL

In Wireless Personal Area Network (WPAN) applications there are essentially two channels of interest: off-body and on-body. The off-body channel is concerned with communication between a device on the body and a remote location. Example applications include short range communications between two soldiers on a battle field or the transmission of medical data from a wireless sensor body area network to a remote station. On-body channels exist where there is a need for communication between devices located on, or within, the user's body. For example, in a telemedicine application where biosensors are implanted in the body, a wearable sensor is often located on the body to act as a relay between the biosensors and a non-local station several meters away from the user. In such applications it is clear that both propagating modes (on-body and off-body) will be required. Furthermore, in a multi-path environment on-body devices may also communicate via EM waves diffracted or reflected from nearby objects. However, in anechoic environments electromagnetic waves may propagate around the body via two mechanisms. One route is penetration directly through the body and the second one is via a creeping wave that follows the body surface. Furthermore, at UHF and higher frequencies penetration through the body is significantly reduced and it is generally held that the main mechanism for propagation around the body is via a creeping wave [8]. Therefore, a low-profile antenna which radiates maximum power tangential to the body surface will be required to maximise coupling between bodyworn devices, thus enhancing over the body surface communication as illustrated in Fig. 1.

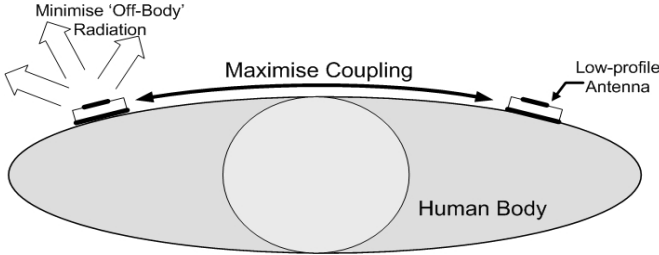


Fig. 1. Sketch of antenna radiation requirements for an 'on-body' channel.

III. ANTENNA GEOMETRY AND SIMULATION SETUP

In this paper, we present the TM_{21}^z mode excited HM-MPA for over the body-surface communication. Such a compact low-profile antenna may be used to replace vertical wire monopoles in on-body communication applications [9]. Fig. 2 shows the geometry of the proposed 2.45 GHz antenna with principle dimensions for free-space operation at the ISM (industrial Scientific and Medical) frequency allocation of 2.4–2.5 GHz. This band is popular for on-body communications because commercial wireless personal area network (WPAN) standards such as Zigbee IEEE 802.15.4 and Bluetooth IEEE 802.15.1 operate there. The 2.45 GHz band is centred at 2442 MHz, with a lower frequency limit of 2400 MHz and an upper frequency one of 2484 MHz.

Therefore, the antenna bandwidth requirement is around 4 % (84 MHz) at the frequency of interest. The HM-MPA consists of a groundplane and patch metallization on a dielectric substrate with a permittivity (ϵ_{r1}) of 2.33 (Taconic TLY-3, PTFE woven glass). The antenna is excited by a top loaded probe at the centre of the patch element [10]. Two posts offset from the feed and shorted to ground are used to force nulls in the tangential electric field component between the groundplane and patch element, exciting a second or higher order resonant mode (TM_{21}^z) [11].

In the FDTD simulation the antenna ground plane and patch element were modelled as a thin sheet of PEC on the dielectric substrate. Both the antenna probe feed and shortening posts were modelled as a thin PEC wire. A sub-cellular approximation is generated by the voxeller in SEMCAD-X for thin sheet and wire bodies rather than a volume representation. This gave a more accurate representation of the thin structure and allowed a larger minimum cell size to be used, directly improving simulation time. A voltage source (edge source) with an internal resistance of 50Ω was used to excite the antenna. For broadband frequency response simulations, a Gaussian sine waveform centred at 2450 MHz with a frequency spectrum from 2 GHz to 3 GHz was used. A non-uniform grid was incorporated in the model to reduce the number of voxel cells required in the computational domain. The maximum cell size near the boundaries of the computational domain was 5 mm ($\lambda/20$). A grid refinement factor of 10 was used on the boundary edges of all solids to ensure appropriate base lines were generated for the model. The minimum cell size at the edges of solids in the computational domain was 0.1 mm. Further grid refinement was applied but did not yield significantly more accurate results for increased simulation time.

Fig. 3 shows normalised current magnitude distribution on the surface of the patch element excited at the higher-order TM_{21}^z mode. Light shaded areas show greatest current magnitude.

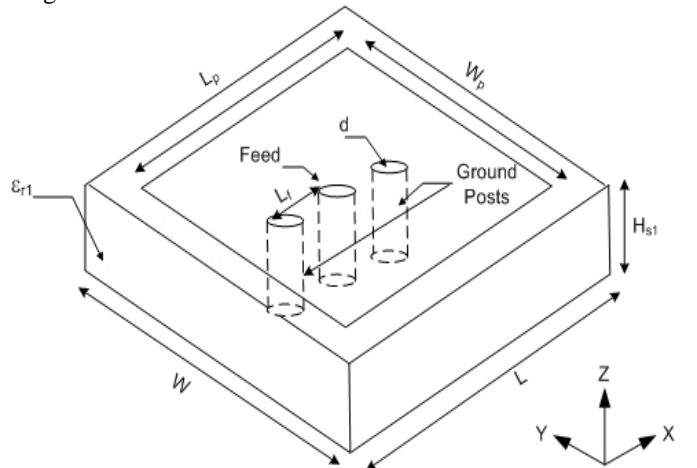


Fig. 2. HM-MPA geometry.

Dimensions for free-space use: $L_p = W_p = 16$ mm; $W = L = 30$ mm; $H_{s1} = 10$ mm; $L_f = 3.3$ mm; $d = 1.2$ mm; $\epsilon_{r1} = 2.33$.

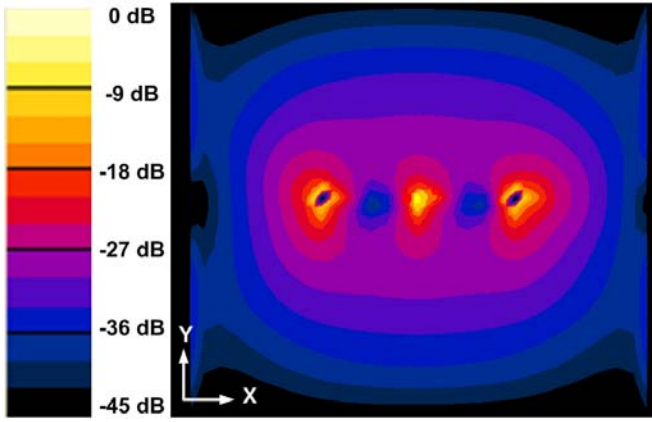


Fig. 3 Normalised current magnitude distribution on the HM-MPA patch.

The simulated co-polar (E_z) far-field radiation patterns for the HM-MPA in free-space at 2442 MHz are shown in Fig. 4. The TM_{21}^z mode radiates an omnidirectional pattern with a directivity of 1.74 dBi similar to that of a circular microstrip antenna excited at the TM_{31} and TM_{41} modes [12]. Fig. 4(a) shows that the HM-MPA radiates mostly in the azimuth plane, with a null in the z-direction and maximum gain in azimuth.

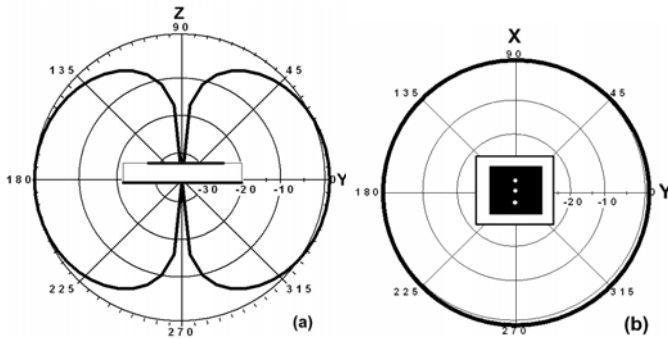


Fig. 4. Simulated co-polar (E_z) far-field radiation patterns for the HM-MPA antenna in free-space: (a) Zenith (YZ plane), (b) Azimuth (XY plane).

IV. HM-MPA ON LOSSY MEDIUM

The dielectric properties of biological tissues vary with both tissue type and frequency. In this study a single 30-mm thick layer of lossy dielectric material was used to represent the user's body. The permittivity and conductivity of the dielectric layer were chosen to represent muscle tissue at 2.44 GHz ($\epsilon = 53.58$, $\sigma = 1.81 \text{ S}^{-1}$) [13]. Fig. 5 shows the simulated S_{11} return loss plots for the HM-MPA under both free space and tissue mounted (1-mm separation) conditions. The antenna was tuned to be resonant at 2.45 GHz on the tissue by appropriately adjusting distance of the ground posts from the centre feed; in this case they were 6.3 mm from the centre. In free space the HM-MPA had an impedance bandwidth of 3.6 % of the resonant frequency for a voltage standing-wave ratio (VSWR) of 2.0 or less, sufficient for the operating bandwidth of the 2.4 GHz WLAN band. When spaced 1 mm from the tissue, the impedance bandwidth increased to 6 %. This bandwidth enhancement is due to the increased coupling losses associated with the lossy medium lowering the antenna Q factor.

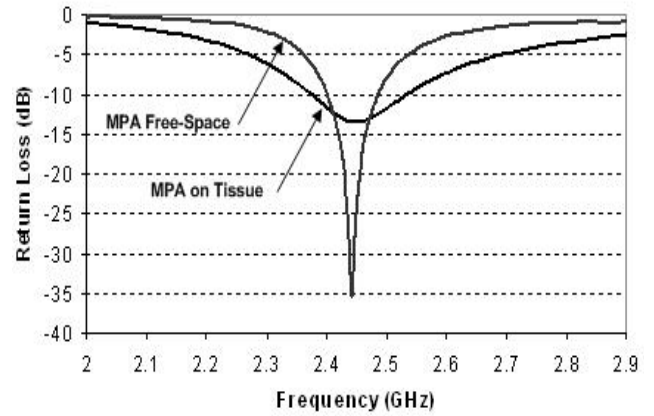


Fig. 5. S_{11} return loss plot for HM-MPA in free-space and mounted 1-mm from a tissue-layer. Dimensions for operation on tissue: $L_p = W_p = 18 \text{ mm}$; $W = L = 30 \text{ mm}$; $H_{s1} = 10 \text{ mm}$; $L_f = 6.3 \text{ mm}$; $d = 1.2 \text{ mm}$; $\epsilon_{r1} = 2.33$.

The far-field radiation patterns in Fig. 4 are informative but they are not particularly relevant to the analysis of antennas for on-body communications where the main mode of propagation is via creeping wave over the body surface. Near-field analysis must be performed to evaluate and improve on-body coupling performance of low-profile antenna structures. Fig. 6 shows the normalised E-field magnitude on a plane normal to the z-axis at the patch surface when the HM-MPA was tissue-mounted. The electric field is symmetrical around the perimeter of the patch element, being equivalent to the fundamental resonant mode, hence the antenna radiates symmetrically around the azimuthal (XY) plane.

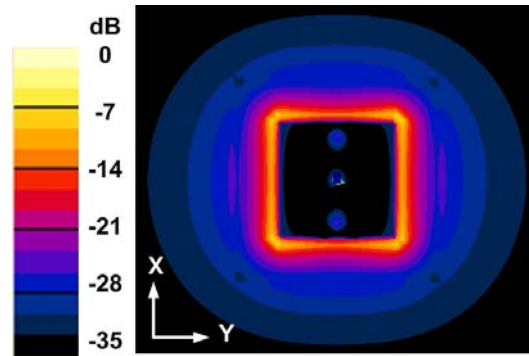


Fig. 6. E-field magnitude distribution on XY plane at patch surface for HM-MPA on tissue.

V. ON-BODY COUPLING RESULTS

The simulation setup used to investigate over-the-body antenna coupling (S_{21}) is shown in Fig. 7. The antennas were spaced 1 mm above and placed 200 mm (D) apart on the flat numerical phantom with dimensions 580 x 380 mm ($L \times W$) respectively. Larger numerical phantoms did not yield substantially more accurate results for increase in computational resource and simulation time. For example, increasing all phantom dimensions by a factor of 2 gave a 0.6 dB change in peak S_{21} values. The transmit antenna (Tx) was excited by voltage source (1 V, impedance 50 Ω). At the receive antenna (Rx) a pure resistive load was placed between the antenna and ground thus enabling calculation of power

delivered to the load from the source (S_{21}). Source sensors at the source and load recorded the received voltage and current as a function of frequency. A SEMCAD-X Python scrip was then used to extract the S_{21} coupling results. The numerical tissue phantom had a height (h) of 30 mm, such that it is larger than the maximum signal penetration depth of muscle tissue at 2.5 GHz [7]. At this frequency the wave penetration into the tissue layer is not significant. Fig. 8 shows the normalised E-field magnitude in a YZ plane through the TX antenna feed point.

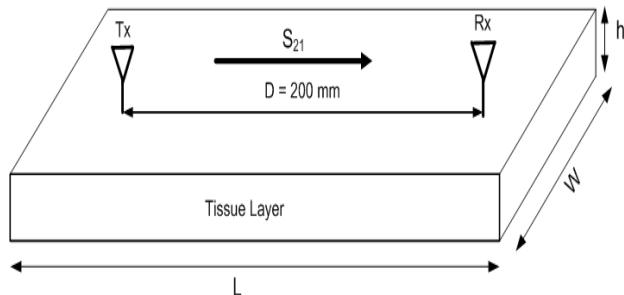


Fig. 7. Antenna coupling simulation setup.



Fig. 8. HM-MPA antenna coupling simulation results showing normalised E-field magnitude through TX feedpoint.

A. HM-MPA On-Body Coupling Performance

The performance of the HM-MPA for on-body coupling was compared to that of a reference monopole antenna. The monopole was modelled as a 0.24λ PEC wire with a diameter of 5 mm mounted on same size of ground plane as the HP-MPA. The impedance bandwidth of the monopole was 343 MHz ($\approx 14\%$) at 2.45 GHz. For comparison, free-space efficiency and tissue proximity efficiency results for both antennas are shown in Table I.

Fig. 9 compares the S_{21} coupling of two HM-MPA antennas for different orientations (detailed in Fig. 10), with two monopole antennas placed 200 mm apart on the tissue layer described above. The key results are then summarised in Table II. The monopole reference antenna and MPA had total tissue proximity losses of 3 dB and 4.2 dB respectively (2 antennas in each measurement scenario). From Table II, the MPA in broadside orientation had 1 dB greater S_{21} coupling loss than the monopole reference antenna. By subtracting total dielectric losses proximity (tissue plus substrate) losses from the S_{21} results, it was estimated that there was a 0.2 dB improvement in coupling loss over the monopole in broadside and 0.8 dB greater loss in end-fire mode for this ‘on-body’ link, as represented by the muscle-equivalent tissue slab.

TABLE I
FREE-SPACE AND TISSUE PROXIMITY EFFICIENCY RESULTS AT 2445 MHz

Antenna	Free-space Efficiency (%)	Tissue-mounted Efficiency (%)	Dielectric losses (tissue & substrate, dB)
Monopole	99	71	2.1
MPA	93	62	1.5

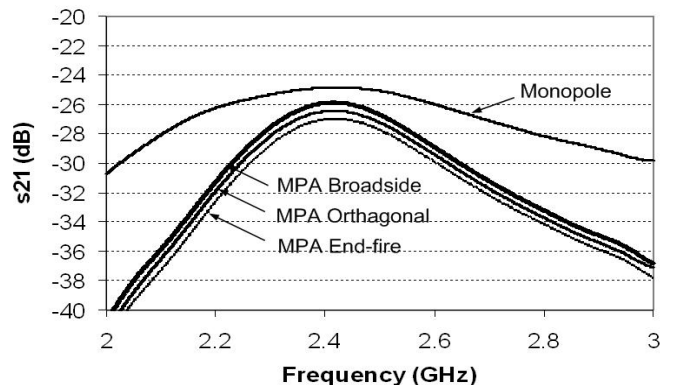


Fig. 9. Simulated S_{21} coupling for HM-MPA versus monopole reference antennas.



Fig. 10. HM-MPA orientation for S_{21} coupling measurements (a) Broadside, (b) Orthogonal and (c) End-fire.

TABLE II
SUMMARY OF S_{21} COUPLING RESULTS OF MPA VERSUS MONOPOLE REFERENCE ANTENNA.

Antenna	Orientation	Peak $ S_{21} $ (dB)	$ S_{21} $ over 3 dB Bandwidth	3 dB Bandwidth
Monopole	-	25.0	28.0	683 MHz
MPA	Broadside	26.0	29.0	348 MHz
MPA	Orthogonal	26.5	29.5	349 MHz
MPA	End-fire	27.0	30.0	345 MHz

B. Effect of Groundplane Size on On-Body Coupling

For a body-mounted patch antenna the size of the groundplane has an important influence on performance. The size of the HM-MPA groundplane was varied from 20 x 20 mm to 40 x 40 mm in 10 mm increments and tissue proximity radiation efficiencies were recorded (Table III). These results show that radiation efficiency increased with an increase in antenna groundplane size. The larger ground plane effectively shields the antenna from the body, hence reducing antenna-body coupling losses, thus increasing antenna efficiency.

Fig. 11 shows the effect of groundplane size on the on-body coupling performance of the HM-MPA (broadside configuration). The results show an improvement in overall S_{21} coupling performance for an increase in ground plane size. This is mainly due to a decrease in tissue losses. There was only a 2% increase in coupling performance by extending the groundplane size to 40 x 40 mm from the 30 x 30mm case.

TABLE III
EFFECT OF GROUND PLANE SIZE ON BODYWORN EFFICIENCY AT
2445 MHz

Ground Plane Size (L x W, mm)	Tissue mounted Efficiency (%)	Dielectric losses (tissue & Substrate, dB)
20 x 20	46.0	3.4
30 x 30	62.0	2.1
40 x 40	66.5	1.8

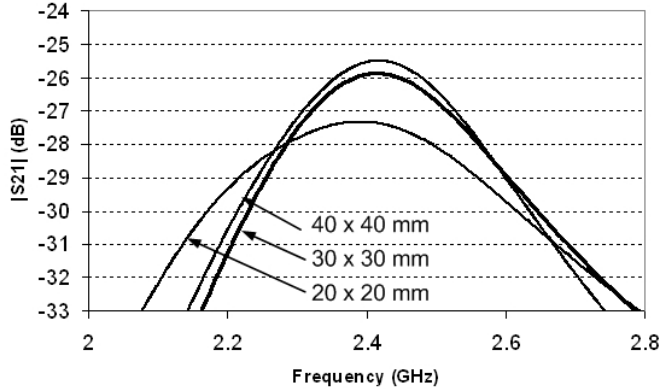


Fig. 11. Effect of ground plane size on S_{21} coupling results for HM-MPA.

C. Effect of Antenna Spacing On On-Body Coupling

Antenna separation distance 'D' (from Fig. 7) was varied up to 400 mm for the MPA (broadside) and monopole reference antenna with S_{21} peak coupling loss recorded at 50 mm intervals (Fig. 12). From Friis' path loss equation, the estimated decay index n was 2.4, slightly higher than the free space value of $n = 2$. However, it is expected that this will significantly increase for more realistic, curved body shapes where the wave propagating across the tissue surface will experience shedding losses.

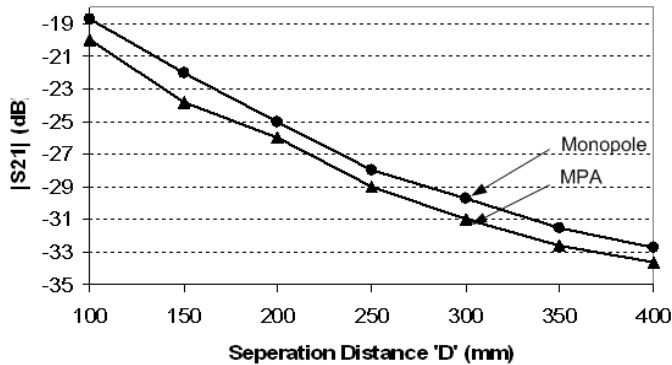


Fig. 12. S_{21} coupling results as a function of antenna separation distance.

VI. CONCLUSION

The on-body coupling performance of a compact microstrip patch antenna excited at a higher-order mode (HM-MPA) in close proximity to a lossy medium has been studied using FDTD at 2.45 GHz. The low-profile antenna has a relatively small ground plane yet provides comparable performance to a full-size monopole. Furthermore, the close proximity to the lossy tissue increased impedance bandwidth by 67%. Therefore, based on its on-body coupling performance, this

low-profile, robust antenna design may be used to replace vertical wire monopoles in on-body communication applications. Future work will include investigation using near-field analysis to improve on-body coupling performance of low-profile antenna structures with a phantom and antenna build to validate simulation results. Antenna height reduction, but with preservation of the impedance bandwidth will be sought for a lower-profile design. The feed technique used to excite the antenna is an important aspect of body-worn antenna design. The proposed antenna can be fed by a quarter wavelength 50Ω microstrip line connected to the bottom of the probe printed on a second substrate layer. Alternative microstrip antenna feed techniques such as insert feed and electromagnetically coupled feed (coupled line, aperture coupled) must be investigated for practical wearable system designs. Subsequent investigations will also include characterisation on a three-layer tissue model (skin, fat and muscle).

REFERENCES

- [1] C.A. Winterhalter, J. Teverovsky, P. Wilson, J. Slade, W. Horowitz, E. Tierney and V. Sharma, "Development of electronic textiles to support networks, communications, and medical applications in future U.S. Military protective clothing systems," *IEEE Trans. Information Technology in Biomedicine*, vol. 9, pp. 402–406, 2005.
- [2] K.L. Wong, C.I. Lin. "Characteristics of a 2.4-GHz compact shorted patch antenna in close proximity to a lossy medium," *Microwave and Optical Technology Letters*, vol. 45, Issue 6, pp. 480–483, 2005.
- [3] B. Sanz-Izquierdo, F. Huang, J.C. Batchelor, "Covert dual-band wearable button antenna," *IEE Electronics Letters*, vol. 42, pp. 3–4, 2006.
- [4] K. Ogawa, T. Uwano and M. Takahashi, "A shoulder-mounted planar antenna for mobile radio applications," *IEEE Trans. Vehicular Technology*, vol. 49, pp. 1041–1044, 2000.
- [5] W.G. Scanlon and N.E. Evans, "Body-surface mounted antenna modelling for biotelemetry using FDTD with homogeneous, two- and three-layer phantoms," in *IEE 10th Intl. Conf. on Antennas & Propagation*, vol.1, pp. 342–345, 1997.
- [6] P. Salonen, Y. Rahmat-Samii, M. Schaffrath and M. Kivikoski, "Effect of textile materials on wearable antenna performance: a case study of GPS antennas," *IEEE Antennas and Propagation Society International Symposium*, pp. 459–462 Vol.1, 2004.
- [7] W.G. Scanlon and N.E. Evans, "Numerical analysis of bodyworn UHF antenna systems," *IEE Electronics & Communication Engineering Journal*, vol. 13, pp. 53–64, 2001.
- [8] J. Ryckaert, P. De Doncker, R. Meys, A. de Le Hoye and S. Donnay, "Channel model for wireless communication around human body," *IEE Electronics Letters*, vol. 40, pp. 543–544, April, 2004.
- [9] L. Economou and R. J. Langley, "Patch antenna equivalent to simple monopole," *Electronic Letters*, vol. 33, no. 9, pp. 727–729, May 1997.
- [10] C. Delaveaud, P. Leveque, and B. Jecko, "New kind of microstrip antenna: The monopolar wire-patch antenna," *Electron. Lett.*, vol. 30, pp. 1–2, Jan. 1994.
- [11] C.A. Balanis, *Advanced Engineering Electromagnetics*. Canada: John Wiley & Sons, 1989, ch. 8.
- [12] J. Huang, "Circularly polarized conical patterns from circular microstrip antennas," *IEEE Trans. Antennas Propagation*, vol. AP-32, pp. 991–994, Sept. 1984.
- [13] FCC, C. Gabriel, "4-Cole-Cole Analysis on Compilation of the Dielectric Properties of Body Tissues at RF and Microwave Frequencies" by Camelia Gabriel, Brooks Air Force Technical Report AL/OE-TR-1996-0037, 1996. Available (<http://www.fcc.gov/fcc-bin/dielec.sh>).